

Modeling of whole process of ageing precipitation and strengthening in Al-Cu-Mg-Ag alloys with high Cu-to-Mg mass ratio

HOU Yan-hui(侯延辉)^{1,2,3}, GU Yan-xia(谷艳霞)^{1,2}, LIU Zhi-yi(刘志义)^{1,2},
LI Yun-tao(李云涛)^{1,2}, CHEN Xu(陈旭)^{1,2}

1. Key Laboratory of Nonferrous Metal Materials Science and Engineering, Ministry of Education, Central South University, Changsha 410083, China;
2. School of Materials Science and Engineering, Central South University, Changsha 410083, China;
3. Key Laboratory for Ferrous Metallurgy and Resources Utilization of Ministry of Education, Wuhan University of Science and Technology, Wuhan 430081, China

Received 12 May 2009; accepted 14 October 2009

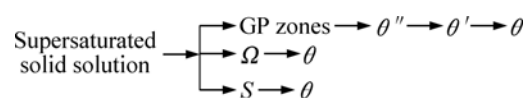
Abstract: A physically based numerical model to predict the microstructure evolution and yield strength of high Cu-to-Mg mass ratio Al-Cu-Mg-Ag alloys during the whole ageing process was developed. A thermodynamically-based precipitation model, employing the classical nucleation and growth theories, was adapted to deal with the precipitation kinetics (evolution of radius and volume fraction of precipitates for Ω phase) of aged Al-Cu-Mg-Ag alloys. The model gives an estimation of the precipitation kinetics (evolution of radius and density of precipitates for both θ' and Ω phases) of the alloy. The strengthening model based on Orowan mechanism was deduced. The microstructural development and strength predictions of the model are generally in good agreement with the experimental data.

Key words: ageing; precipitation; modeling; microstructure; thermodynamics; strengthening

1 Introduction

In recent years, much effort has been devoted to model the precipitation kinetics and the relationship between the precipitation microstructure and the resulting mechanical properties[1–9]. Al-Cu-Mg-Ag alloys with high Cu-to-Mg mass ratio are promising candidates for applications in elevated temperature aerospace industry. By adding a small amount of Mg and Ag in traditional Al-Cu alloys, thin, hexagonal-shaped plate-like particles of a new phase, designated as Ω phase, form uniformly on the {111} planes of matrix, thereby high-temperature mechanical performances are significantly improved[10–11]. Although there is a lot of problem to be understood, many researches described the precipitation mechanism of Ω phase, and agreed that Mg-Ag clusters acted as the nucleation sites for Ω phase[12–14]. Precipitation of Al-Cu-Mg-Ag alloy relies upon the ageing process and alloy composition greatly. Effect of ageing temperature on precipitation of ageing

hardened alloys had been studied in detail in Ref.[15]. According to layered structure of Ag-Mg co-clusters, amount of Ag added, as well as the molar ratio of Ag to Mg, had been researched[11, 16]. Based on EMR (elements mass ratio) technique in Ref.[17], the mass ratio of principal solute atoms in heat-resistant Al-Cu-Mg-Ag alloys got to be designed as $w(\text{Cu})/w(\text{Mg}) \approx 10$, $w(\text{Ag})/w(\text{Mg}) \approx 1$ and $w(\text{Mg})/w(\text{Si}) > 10$, which could promote the formation of Ω phase and its thermal stability. We assumed that the content of Mg-Ag co-clusters was sufficient to facilitate the nucleation of Ω phase for these alloys designed above. Consequently, only Cu solute atoms were considered in the solute mass conservation equation. The microstructural evolution for this kind of alloys would involve the following three main processes:



Formation of GP zones and θ'' precipitates is quite

rapid and likely to precede the precipitation of the Ω phase. As the ageing time increases, the proportion of phases on $\{001\}_\alpha$ diminishes and this Cu solute is consumed by further nucleation and growth of a fine dispersoid of the Ω phase on $\{111\}_\alpha$, which becomes the dominant precipitate. The S phase was not observed in this study due to high Cu-to-Mg ratio. So, only Ω phase was considered in this article.

The activation energy for homogeneous nucleation consists of three parts[18], namely, the chemical free energy arising from the chemical supersaturation of the solutes, the interfacial energy spent for creating the precipitate/matrix interface and the strain energy used to accommodate the strain mismatch. And according to Refs.[15, 19–21], Ω phase was coherent. Consequently, the strain energy part is neglected in order to reduce the complexity in the present case. This hypothesis has been successfully employed in many earlier works[1, 4, 9] based on Kampmann and Wagner (KW) model.

According to Ref.[22], Mg and Ag are not incorporated within the platelet, and its chemical composition is Al-33%Cu (molar fraction). Consequently, we assumed that the stable nuclei of a critical radius did not incorporate Cu atoms.

In this work, based on the established interfacial energy model, pseudo-binary assumption and the classical nucleation and growth theories, a thermodynamically based precipitation model was established to describe precipitation kinetics of Ω phases in aged Al-Cu-Mg-Ag alloys. This approach had been applied to predict evolution of radius and volume fraction of the strengthening particles. Then, strengthening model based on Orowan mechanism was established to predict yield strength.

2 Model

The modeling of precipitation kinetics is based on the Kampmann and Wagner (KW) type numerical model, which has been used by several researchers[6]. The model is formulated in a pseudo-binary approximation. Mg and Mg-Ag co-clusters facilitate the nucleation of Ω phases by reducing interfacial energy of the precipitate nuclei. Expanding the model to four components (Al, Cu, Mg, Ag) is possible by considering Mg and Ag concentrations as an efficiency factor in precipitate/matrix interfacial energy. The model is based on homogeneous precipitation.

2.1 Thermodynamic model

An ideal solution model is considered. Activity of the atomic species is characterized by their concentrations. The driving force at any time can be written as[22]

$$\Delta g = -\frac{kT}{V_{\text{at}}} \left[C_p \ln \left(\frac{C}{C_{\text{eq}}} \right) + (1 - C_p) \ln \left(\frac{1 - C}{1 - C_{\text{eq}}} \right) \right] \quad (1)$$

where V_{at} is the atomic volume; k is the gas constant; T is the temperature; C_{eq} is the equilibrium solute concentration of the matrix; C is the current solute concentration of the matrix; and C_p is the solute concentration at the equilibrium precipitate/matrix interface.

From this driving force, a critical radius R^* can be derived for the precipitates at a given solute concentration C :

$$R^* = -\frac{R_0}{C_p \ln \left(\frac{C}{C_{\text{eq}}} \right) + (1 - C_p) \ln \left(\frac{1 - C}{1 - C_{\text{eq}}} \right)} \quad (2)$$

where $R_0 = 2\gamma V_{\text{at}} / (kT)$, and it is a thermodynamic parameter which has the dimension of a length. R^* is identified as critical radius, above which the probability for the atoms in nucleation site to break away derived by heat fluctuating is small enough, and the precipitates begin to nucleate and grow up into new particles; below which the dissolution stage appears. γ is the precipitate/matrix interfacial energy.

The energy for nucleation, which is defined as the smallest activation energy barrier ΔG^* , is the energy for precipitates to reach the critical radius. The most effective way to minimize ΔG^* is to form nucleus, which has the minimum interfacial energy:

$$\Delta G^* = \frac{16}{3} \pi \frac{\gamma^3}{\Delta g^2} \quad (3)$$

2.2 Nucleation, growth and coarsening

In the first stage, nucleation and growth were considered to take place at the same time. The nucleation rate is calculated via the classical Becker-Doring theory, and the precipitates density is given by the nucleation rate. The nucleation rate can be written as[23–24]

$$\frac{dN}{dt} = N_0 Z \beta^* \exp \left(-\frac{\Delta G^*}{KT} \right) \exp \left(-\frac{\tau}{t} \right) \quad (4)$$

where N is the precipitate density; N_0 is the number of atoms by unit volume ($=1/V_{\text{at}}$); t is the time; Z is Zeldovich's factor; K is the Boltzman constant; $\beta^* = 4\pi R^{*2} DC/a^4$; D is the diffusion coefficient of solute atoms in the matrix; and a is the lattice parameter of the precipitate. Before the start of the general transformation there is an incubation time $\tau = 1/(2\beta^* Z)$. τ is infinitesimal, so $\exp(-\tau/t) \approx 1$.

The evolution of the mean precipitate radius is given by the combination of the growth of existing precipitates and the arrival of new precipitates at the

nucleation radius R^* [25–26]:

$$\frac{dR}{dt} = \frac{D}{R} \frac{C - C_{eq} \exp(R_0/(C_p R))}{C_p - C_{eq} \exp(R_0/(C_p R))} + \frac{1}{N} \frac{dN}{dt} (\alpha R^* - R) \quad (5)$$

The numerical factor α accounts for the fact that nucleated precipitates can grow only if their radii are slightly larger than the nucleation radius. $\alpha=1.05$ has been taken in this work[1].

The whole process follows the equation of solute conservation:

$$C = C_0 - \frac{4}{3} \pi C_p N(R)^3 \quad (6)$$

where C_0 is the initial solute concentration. Pure solution is assumed in the precipitates, i.e. $C_p=1$.

Only when the mean precipitation radius is larger than the critical radius, can the free energy decrease and the precipitates begin to grow. The equations describing the growth stage is[26]:

$$\frac{dN}{dt} = 0 \quad (7)$$

$$\frac{dR}{dt} = \frac{D}{R} \frac{C - C_{eq} \exp(R_0/(C_p R))}{C_p - C_{eq} \exp(R_0/(C_p R))} \quad (8)$$

When the mean radius and the critical radius are equal, the conditions for the standard LSW law are fulfilled[27]:

$$\frac{dR}{dt} = \frac{4}{27} \frac{C_{eq}}{1 - C_{eq}} \frac{R_0 D}{R^2} \quad (9)$$

$$\frac{dC}{dt} = - \frac{R_0 C}{R^2} \frac{dR}{dt} \quad (10)$$

The calculation of the derivative of Eq.(6) with respect to t gives the rate of variation of the density of precipitates in pure coarsening:

$$\frac{dN}{dt} = - \frac{1}{\pi A C_p R^3} \left(\frac{dC}{dt} + 3\pi A C_p N R^2 \frac{dR}{dt} \right) \quad (11)$$

2.3 Modeling of yield strength

The precipitates are considered to be nonshearable, and hence strengthening is based on the Orowan looping mechanism. The increment of yield strength arisen by the $\{111\}_\alpha$ -plates yields[28]

$$\Delta\tau_\Omega = 0.12MG \frac{b}{2\sqrt{rh}}$$

$$\left[\varphi^{1/2} + 0.70 \left(\frac{r}{h} \right)^{1/2} \varphi + 0.12 \left(\frac{r}{h} \right) \varphi^{3/2} \right] \ln \left(\frac{0.158r}{r_0} \right) \quad (12)$$

where M is the Taylor factor. G is the shear modulus. b is the magnitude of the Burgers vector. r and h ($\ll r$) are

radius and thickness of the plate, respectively. φ is the volume fraction and the equation is $\varphi = \frac{2\pi r^3}{A} N_0 Z \beta^* \exp\left(\frac{-\Delta G^*}{KT}\right) t$. r_0 is the inner cut-off radius for the calculation of the dislocation line tension.

When calculating the yield stress, one needs finally to add the contribution of solute hardening, precipitation hardening and dislocation hardening[29–30]:

$$\tau_y = \tau_0 + \Delta\tau_{sol} + \sqrt{\Delta\tau_\Omega^2 + \Delta\tau_d^2} \quad (13)$$

where τ_y is the total yield strength. τ_0 is the intrinsic strength of aluminum. $\Delta\tau_{sol}$ is the contribution from the solid solution to the yield strength. $\Delta\tau_\Omega$ is the contribution from Ω phase to the yield strength. And $\Delta\tau_d$ is the dislocation contribution to the yield strength.

The input parameters used in the models above are summarized in Table 1.

Table 1 Parameters in model

Parameter	Value	Comment	Reference
$V_{al}/(\text{m}^3 \cdot \text{mol}^{-1})$	2.83×10^{-5}	Molar volume of precipitates	[1]
Z	$\approx 1/20$	Zeldovich factor	[31]
a/nm	0.404	Lattice parameter of Al-matrix	[32]
$D/(\text{m}^2 \cdot \text{s}^{-1})$	$6.0 \times 10^{-6} \times \exp(-119691/kT)$	Diffusion coefficient	[33]
$A/(\text{r} \cdot \text{h}^{-1})$	20	Aspect ratio	[34]
M	3.1	Magnitude of Taylor factor	[35]
$G/(\text{N} \cdot \text{m}^{-2})$	2.8×10^{10}	Magnitude of shear modulus	[28]
b/m	0.286×10^{-9}	Magnitude of Burgers factor	[28]
r_0/m	2b	Inner cut-off radius	[28]

3 Experimental

The composition (mass fraction, %) of the alloys used is shown in Table 2. After continuous casting, the rectangular ingot was homogenized at 500 °C for 6 h followed by air cooling to room temperature. The ingot was then scalped and rolled at 450 °C into thin plate with a rectangular section of 130 mm × 2 mm. Specimens for mechanical properties test were prepared in L-T direction of the thin plate with gauge length of 30 mm. The specimens were solution treated for 6 h at 505 °C, quenched in water at room temperature and then immediately aged at different temperatures with different ageing time. Differential scanning calorimetry (DSC)

analysis in different heating rate (5, 10 and 20 °C/min) was operated on the NETZSCH STA 449C thermal analyser after the solution treatment. The specimen for DSC analysis was thin slices of 5 mm in diameter. TEM samples were thin slice with 3 mm in diameter and electro-polished by using twin-jet equipment with a voltage of 10 V in a 70% ethanol and 30% nitric acid at approximately -20 °C. These samples were then examined in a Tecnai G² 20 ST TEM machine operating at 200 kV. Mechanical property tests were performed at room temperature on the CSS-44100 type testing machine with a cross-head speed of 2 mm/min. The experimental data reported in this work are the mean values of three specimens which are in the same tempered condition.

Table 2 Alloys composition (mass fraction, %)

Cu	Mg	Ag	Mn	Fe	Si	Al
6.2	0.6	0.51	0.3	0.04	0.01	Bal.

4 Simulation result and discussion

4.1 Model parameters

4.1.1 Interfacial energy

The sensitivity of the thermodynamic models to interfacial energy is very high because exponent of the interfacial energy entered in the activation energy is 3[9]. The interfacial energy is obtained by fitting the model predictions to the experimental results, which has been employed in many literatures based on the KW model[9].

Mg and Mg-Ag co-clusters facilitate the nucleation of Ω by reducing interfacial energy of the precipitate nuclei. These elements influence the nucleation of the Ω phase (Ag-Mg co-clusters nucleated Ω phase) and then affect the growth of this phase (segregate at the interface with Al). Therefore, the interfacial energy for nucleation of Ω phase is likely to be different from the interfacial energy for its growth. The change of interfacial energy is more important in nucleation stage than in growth stage. So, the interfacial energy of growth stage is the terminative value of nucleation and growth stage in this work.

When the concentration of Mg and Ag changed, the same method was used to fit the interfacial energy for another alloy. Consequently, the effect of Mg and Ag concentrations on interfacial energy was taken into account. The interfacial energy within the nucleation and growth regime for the alloy studied in this work is taken as the following equation, which provided the best results:

$$\gamma_{\Omega} = 0.20 - (-6.13 \times 10^{-14} T^3 + 1.98 \times 10^{-11} T^2 - 1.72 \times 10^{-9} T) t \quad (14)$$

4.1.2 Equilibrium solute concentration of matrix

The equilibrium solute mole fraction with Ω phase in the matrix is difficult to measure experimentally and no values are available in the literature. The following equation is employed:

$$C_{\text{eq}}^{\Omega} = k_{\text{eq}}^{\Omega} \exp\left(-\frac{\Delta H_{\Omega}}{RT}\right) \quad (15)$$

where k_{eq}^{Ω} is a constant which is derived by considering that the stability limit of Ω phase in Al-Cu-Mg-Ag alloy is 550 °C [36]. ΔH_{Ω} represents the enthalpy of formation of one mole of Ω phase. It can be obtained by following Ref.[11]. DSC curves of the solution treated and quenched alloy at varying heating rates are shown in Fig.1. Three peaks marked with A1, A3 and A4 are exothermic peaks, and A2 is endothermic peak. According to the precipitation sequence of high Cu-to-Mg mass ratio Al-Cu-Mg-Ag alloys, these exothermic peaks correspond to the formation of GP zones and Ag-Mg co-clusters, Ω phases, θ' phase, respectively. And endothermic peaks correspond to the dissolution of GP zones.

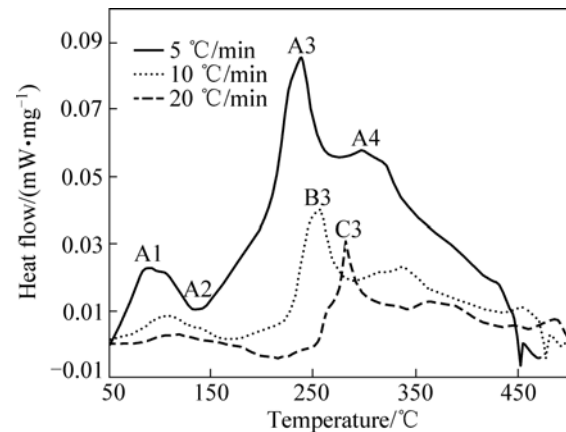


Fig.1 DSC curves of solution treated and quenched alloy at varying heating rates

From a regular solution model, we obtain the solid solubility of element Cu:

$$c_{\text{Cu}} = c_0 \exp[\Delta H_{\Omega} / k_B T] \quad (16)$$

ΔH_{Ω} value relies on precipitation effects observed in DSC curves. The end of precipitation effect should occur when the composition of the matrix around the precipitate reaches the equilibrium:

$$\Delta Q = \Delta H_{\Omega} (x_{0-\text{Cu}} - c_{\text{Cu}}) \quad (17)$$

where $x_{0-\text{Cu}}$ is the initial concentration of Cu. c_{Cu} is the solid solubility of Cu (in molar fraction). Fitting the data of A1, A3, A4 at different heating rates from the DSC curves (Fig.1) using Eqs. (17) and (18), the enthalpy of formation of Ω phase was obtained. The two equations can be written in the following form:

$$\begin{aligned} \Delta Q &= \Delta H_{\Omega}(x_{0_Cu} - c_{Cu}) \\ &= \Delta H_{\Omega}(x_{0_Cu} - c_1 \exp(\Delta H_{\Omega} / k_B T)) \end{aligned} \quad (18)$$

ΔQ_A , ΔQ_B and ΔQ_C were calculated to be 18, 20 and 27 J/g, respectively. The overlap between A2 and A3 was not considered in this work. The enthalpy of formation of Ω phase was $\Delta H_{\Omega}=32\ 863$ J/mol.

4.1.3 Other parameters

Because of the effect of texture, the values of M are different in different directions. In this work, the direction of yield strength is transverse. According to Ref.[35], 3.1 is adopted. In the present alloys, the composition of Ω precipitate is Al_2Cu , So, V_{at} is the molar volume of precipitates. Design of the alloys in this work ensures that the content of Mg-Ag co-clusters is large enough to precipitate phase sufficiently, and the KW model in this work is based on pseudo-binary assumption. Composition of the precipitate is Al_2Cu , while Ag and Mg are not contained. Furthermore, the fraction of solute atoms of Cu among the three elements is the largest. Consequently, D is diffusion coefficient of Cu solute atom in matrix. $A(=r/h)$ is taken as 20 for plate precipitate in this work.

4.2 Evolution of microstructure

Fig.2 shows the evolution of precipitates radius, critical radius and volume fraction of the alloy aged at 165, 200 and 250 °C. $R(\Omega)$ and $R^*(\Omega)$ are the mean radius and the critical radius of of Ω phase respectively, and $\varphi(\Omega)$ is the transformed volume fraction of Ω phase. Because the diffusion of Cu atoms on $\{111\}_\alpha$ is encumbered by the diffusion of Mg and Ag atoms on it, the growth rate of Ω phase is much smaller. As ageing time prolongs, precipitations on the $\{001\}_\alpha$ are consumed by further precipitation of Ω phases. At that time, the solute concentration is not necessary to be zero. Ω phases continue to grow until the mean radius of Ω phases reaches the critical radius. By comparing Fig.2(a) with Fig.2(b) and Fig.2(c), it can be seen that as the ageing temperature increases, the growth rate of precipitates is increased, so the radius of the precipitates is also increased. Consequently, time for the precipitates to reach the critical radius is shortened in turn. At the same time, the presence of Mg and Ag atoms on the Ω/α interface reduces the lattice distortion energy, so Ω plates have high stability at high ageing temperature. The predicted radius of the Ω phase formed during isothermal treatment has been demonstrated by experimentally results of the precipitate radius measured according to TEM micrographs in Fig.3. The predicted radius and the experimental results are presented in Table 3. It is observed that the predicted radius and transformed volume fraction of the precipitates correspond well with the measured results.

4.3 Simulated results of yield strength

Fig.4 shows that the predicted values of yield strength are in good agreement with the experimental results. This demonstrates the physical model established above has a high accuracy in prediction.

As shown in Fig.4, according to the ageing temperature, the age response time of the peak-age condition is different. The higher the temperature is, the shorter the time is needed to the peak-age, while the peak strength value is smaller. It is known that the nucleation,

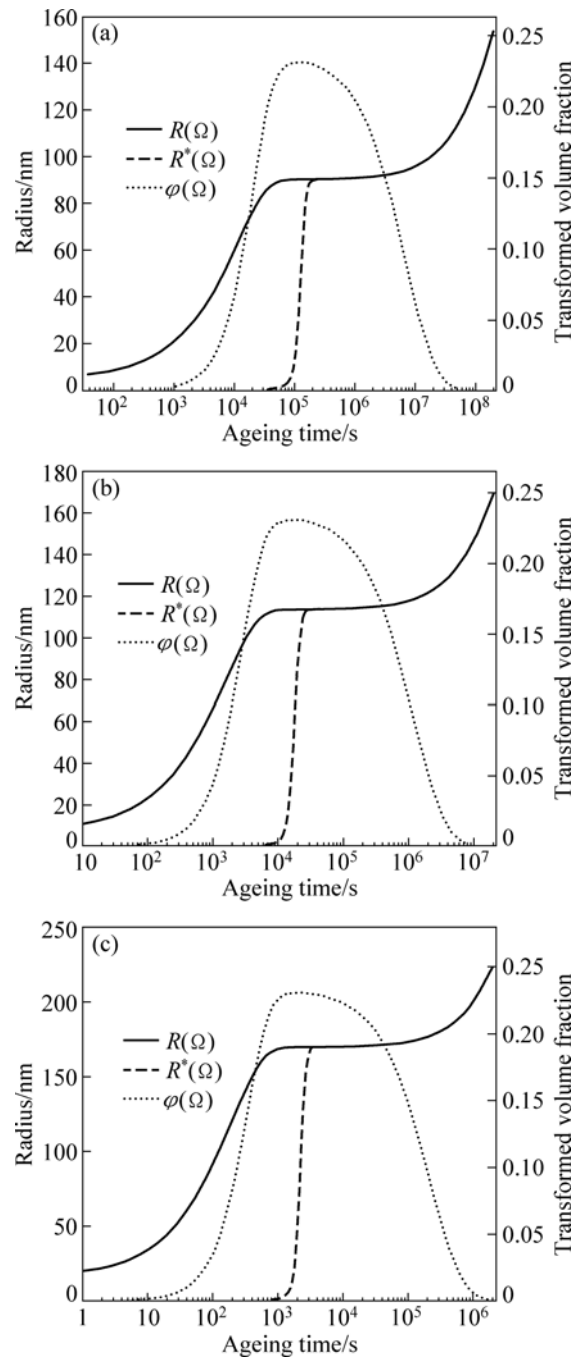


Fig.2 Evolution of radius and transformed volume fraction of Ω phase of Al-Cu-Mg-Ag alloy aged at different temperatures: (a) 165 °C; (b) 200 °C; (c) 250 °C

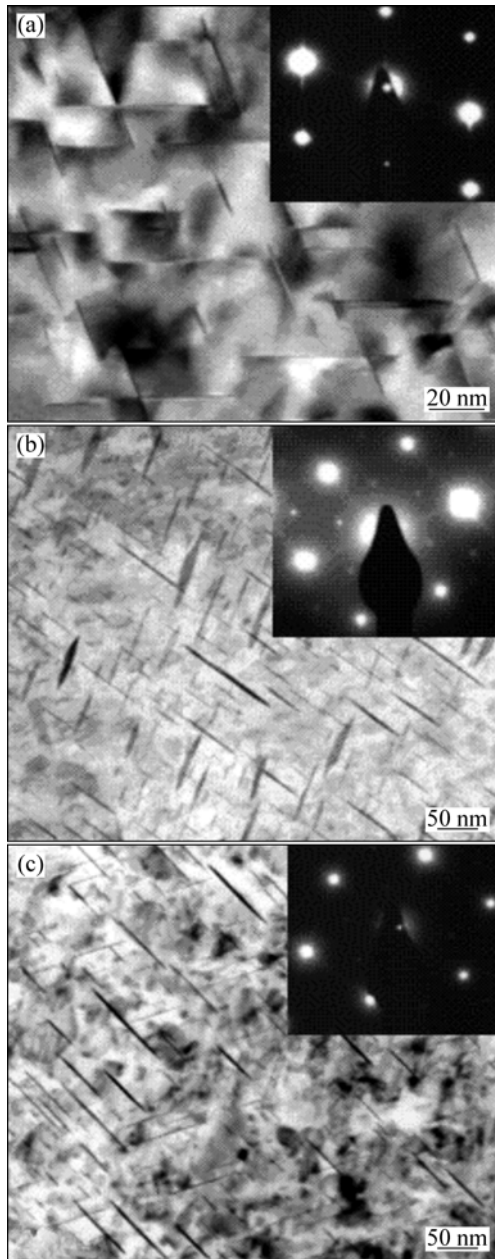


Fig.3 TEM images of precipitates of alloy in different peak ageing conditions and corresponding diffraction spots: (a) 165 °C, 10 h; (b) 200 °C, 4 h; (c) 250 °C, 10 min

Table 3 Comparison of predicted size and measured one from TEM images of precipitates

Ageing treatment	Radius of Ω precipitates/nm		Volume fraction of Ω precipitates	
	Predicted	Measured	Predicted	Measured
165 °C, 10 h	88.25	80.77	0.25	0.22
200 °C, 4 h	113.51	102.33	0.23	0.24
250 °C, 10 min	153.39	139.93	0.22	0.28

growth and coarsening of the precipitates are relative to the diffusion of vacancies and solute atoms. According to the Arrhenius equation, $D=D_0\exp(-Q/RT)$, the diffusion

velocity is greatly influenced by temperature. The supersaturated solid solution decomposes faster with high diffusion coefficient in higher ageing temperature and the precipitates grow more quickly by absorbing the solute atoms nearby, leading to the peak-age appearing earlier. Precipitates absorb atoms nearby to grow up rapidly at higher ageing temperature, and the solute atoms around are poor and cannot form new precipitates. Consequently, the peak strength decreases as a result of the decrease of precipitates density when ageing temperature is increased.

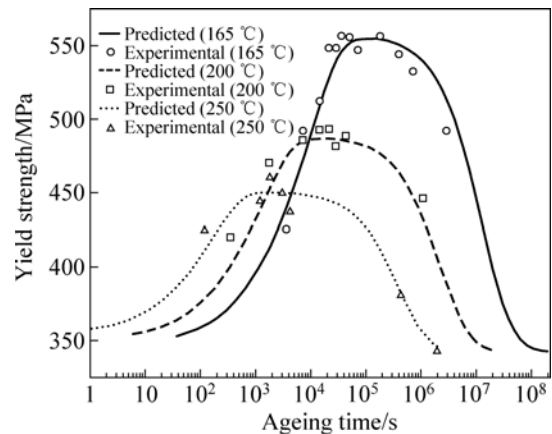


Fig.4 Experimental results and model predictions of yield strength for alloy aged at different temperatures

5 Conclusions

1) A numerical model based on the Kampmann and Wagner model has been developed for predicting precipitation of Ω phases in ageing process of Al-Cu-Mg-Ag alloys. It can predict evolution of precipitate radius and volume fraction of Ω phases.

2) The strengthening model based on Orowan mechanism is deduced. The analytical method and the micro-structural models have been validated by the excellent agreement between the predicted values and the results from related quantitative TEM studies and the yield strength data.

References

- [1] DESCHAMPS A, BRECHET Y. Influence of predeformation and ageing of an Al-Zn-Mg alloy: II. Modeling of precipitation kinetics and yield stress [J]. *Acta Materialia*, 1998, 47(1): 293–305.
- [2] MYHR O R, GRONG O, ANDERSEN S J. Modelling of the age hardening behaviour of Al-Mg-Si alloys [J]. *Acta Materialia*, 2001, 49(1): 65–75.
- [3] MYHR O R, GRONG Ø, FJÆR H G, MARIOARA C D. Modelling of the microstructure and strength evolution in Al-Mg-Si alloys during multistage thermal processing [J]. *Acta Materialia*, 2004, 52(17): 4997–5008.
- [4] STARINK M J, WANG S C. A model for the yield strength of

- Al-Zn-Mg-Cu alloys [J]. *Acta Materialia*, 2003, 51(17): 5131–5150.
- [5] WANG S C, LEFEBVRE F, YAN J L, SINCLAIR I, STARINK M J. VPPA welds of Al-2024 alloys: Analysis and modelling of local microstructure and strength [J]. *Materials Science and Engineering A*, 2006, 431(1/2): 123–136.
- [6] ROBSON J D, JONES M J, PRANGNELL P B. Extension of the N-model to predict competing homogeneous and heterogeneous precipitation in Al-Sc alloys [J]. *Acta Materialia*, 2003, 51(5): 1453–1468.
- [7] ROBSON J D. A new model for prediction of dispersoid precipitation in aluminium alloys containing zirconium and scandium [J]. *Acta Materialia*, 2004, 52(6): 1409–1421.
- [8] LIU G, ZHANG G J, DING X D, SUN J, CHEN K H. Modeling the strengthening response to ageing process of heat-treatable aluminum alloys containing plate/disc- or rod/needle-shaped precipitates [J]. *Materials Science and Engineering A*, 2003, 344(1/2): 113–124.
- [9] KHAN I N, STARINK M J, YAN J L. A model for precipitation kinetics and strengthening in Al-Cu-Mg alloys [J]. *Materials Science and Engineering A*, 2008, 472(1): 66–74.
- [10] TAYLOR J A, PARKER B A, POLMEAR I J. Precipitation in Al-Cu-Mg-Ag casting alloy [J]. *Metal Science*, 1978, 12(10): 478–482.
- [11] CHESTER R J, POLMEAR I J. Abnormal age hardening in an Al-Cu-Mg alloy containing silver and lithium [J]. *Scripta Materialia*, 1989, 23(7): 1213–1217.
- [12] MURAYAMA M, HONO K. Three dimensional atom probe analysis of pre-precipitate clustering in an Al-Cu-Mg-Ag alloy [J]. *Scripta Materialia*, 1998, 38(8): 1315–1319.
- [13] REICH L, MURAYAMA M, HONO K. Evolution of Ω phase in an Al-Cu-Mg-Ag alloy—a three-dimensional atom probe study [J]. *Acta Materialia*, 1998, 46(17): 6053–6062.
- [14] FERRAGUT R, DUPASQUIER A, MACCHI C E, SOMOZA A, LUMLEY R N, POLMEAR I J. Vacancy–solute interactions during multiple-step ageing of an Al-Cu-Mg-Ag alloy [J]. *Scripta Materialia*, 2009, 60(1): 137–140.
- [15] MUKHOPADHYAY A K. On the nature of the second phase particles present in an as-cast Al-Cu-Mg-Ag alloy [J]. *Scripta Materialia*, 1999, 41(6): 667–672.
- [16] ZAHRA A M, ZAHRA C Y, DUMONT M. Effects of Ag or Si on precipitation in the alloy Al-2.5 mass% Cu-1.5 mass% Mg [J]. *Philosophical Magazine*, 2005, 85(31): 3735–3754.
- [17] LI Yun-tao. Microalloying mechanism and performance characterizing of Al-Cu-Mg-Ag alloys with Er, Sc and Ce added [D]. Changsha: Central South University, 2008.
- [18] DUTTA B, PAMIERE E J, SELLARS C M. Modelling the kinetics of strain induced precipitation in Nb microalloyed steels [J]. *Acta Materialia*, 2001, 49(5): 785–794.
- [19] LUMLEY R N, MORTON A J, POLMEAR I J. Enhanced creep performance in an Al-Cu-Mg-Ag alloy through underageing [J]. *Acta Materialia*, 2002, 50(14): 3597–3608.
- [20] XIAO D H, WANG J N, DING D Y, CHEN S P. Effect of Cu content on the mechanical properties of an Al-Cu-Mg-Ag alloy [J]. *Journal of Alloys and Compounds*, 2002, 343(1/2): 77–81.
- [21] HONO K, MURAYAMA M, REICH L. Evolution of Ω phase in an Al-Cu-Mg-Ag alloy—A three-dimensional atom probe study [J]. *Acta Materialia*, 1998, 46(17): 6053–6062.
- [22] KAMPMANN R, WAGNER R. Homogeneous second phase precipitation [J]. *Materials Science and Technology*, 1991, 5(6): 213–304.
- [23] VOLMER M, WEBER A. Nuclei formation in supersaturated states [J]. *Physical Chemistry Chemical Physics*, 1926, 119(4): 277–301.
- [24] RUSSELL K C. Nucleation in solids: The induction and steady-state effects [J]. *Advances in Colloid and Interface Science*, 1980, 13(3/4): 205–318.
- [25] ZENER C J. Theory of growth of spherical precipitates from solid solution [J]. *Journal of Applied Physics*, 1949, 20(10): 950–953.
- [26] AARON H B, FAINSTAIN D, KOTLER G R. Diffusion-limited phase transformations: A comparison and critical evaluation of the mathematical approximations [J]. *Journal of Applied Physics*, 1970, 41(11): 4404–4410.
- [27] LIFSHTIZ I M, SLYOZOV V V. The kinetics of precipitation from supersaturated solid solutions [J]. *Journal of Physics and Chemistry of Solids*, 1961, 19(1/2): 35–50.
- [28] LIU Gang, ZHANG Guo-jun, DING Xiang-dong, CHEN Jun, CHEN Kang-hua. A model for age strengthening of Al alloys with plate/disc-like or rod/needle-like precipitate [J]. *Rare Metal Materials and Engineering*, 2003, 32(12): 971–975. (in Chinese)
- [29] GENEVOIS C, DESCHAMPS A, DENQUIN A. Quantitative investigation of precipitation and mechanical behaviour for AA2024 friction stir welds [J]. *Acta Materialia*, 2005, 53(8): 2447–2458.
- [30] NEMBACH E, NEITE A. Precipitation hardening of superalloys by ordered γ' -particles [J]. *Progress in Materials Science*, 1985, 29(3): 177–319.
- [31] LIFSHTIZ I M, SLYOZOV V V. The kinetics of precipitation from supersaturated solid solutions [J]. *Journal of Physics and Chemistry of Solids*, 1961, 19(1): 35–50.
- [32] KING F. *Aluminum and its alloys* [M]. Chichester: Ellis Horwood Limited, 1987.
- [33] BEYELER M, MAURICE M, SEGUIN R. Contribution to study of hetero-diffusion in aluminum [J]. *Mem Sci Rev Metall*, 1970, 67(6): 295–302.
- [34] BOYD J D, NICHOLSON R B. A calorimetric determination of precipitate interfacial energies in two Al-Cu alloys [J]. *Acta Materialia*, 1971, 19(10): 1101–1109.
- [35] HARGARTER H, LYTTLE M T, STARKE E A. Effects of preferentially aligned precipitates on plastic anisotropy in Al-Cu-Mg-Ag and Al-Cu alloys [J]. *Materials Science and Engineering A*, 1998, 257(1): 87–99.
- [36] LI Q, SHENOY R N. DSC and TEM characterizations of thermal stability of an Al-Cu-Mg-Ag alloy [J]. *Journal of Materials Science*, 1997, 32(13): 3401–3406.

(Edited by YANG Bing)